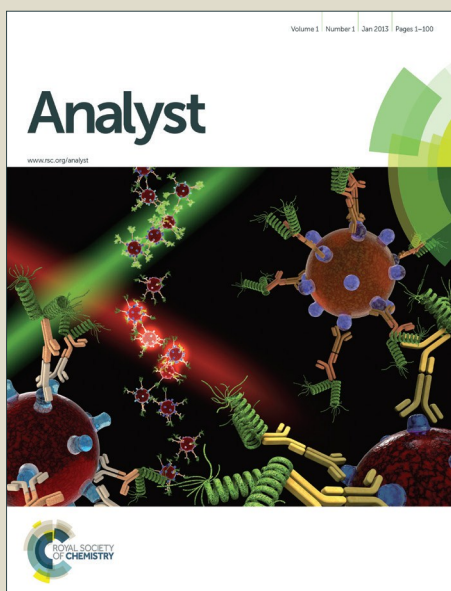


# Analyst

Accepted Manuscript



This is an *Accepted Manuscript*, which has been through the Royal Society of Chemistry peer review process and has been accepted for publication.

*Accepted Manuscripts* are published online shortly after acceptance, before technical editing, formatting and proof reading. Using this free service, authors can make their results available to the community, in citable form, before we publish the edited article. We will replace this *Accepted Manuscript* with the edited and formatted *Advance Article* as soon as it is available.

You can find more information about *Accepted Manuscripts* in the [Information for Authors](#).

Please note that technical editing may introduce minor changes to the text and/or graphics, which may alter content. The journal's standard [Terms & Conditions](#) and the [Ethical guidelines](#) still apply. In no event shall the Royal Society of Chemistry be held responsible for any errors or omissions in this *Accepted Manuscript* or any consequences arising from the use of any information it contains.

# Illustration of surface-induced dissociation (SID)-ion mobility-SID mass spectrometry: homo and hetero model protein complexes.

Royston S. Quintyn,<sup>†</sup> Sophie R. Harvey,<sup>†\*</sup> Vicki H. Wysocki<sup>†</sup>

<sup>†</sup> Department of Chemistry and Biochemistry, Ohio State University, 484 W. 12th Ave., Columbus, Ohio 43210

\* School of Chemistry, Manchester Institute of Biotechnology, University of Manchester, Manchester, M1 7DN, UK

## Table of Contents entry



Surface collisions generate subcomplexes, which are then separated by ion mobility and dissociated into their individual subunits via a second stage of surface collisions to elucidate protein complex architecture and assembly.

## Abstract

The direct determination of the overall topology and inter-subunit contacts of protein complexes plays an integral role in understanding how different subunits assemble into biologically relevant multisubunit complexes. Mass spectrometry has emerged as a useful structural biological tool because of its sensitivity, high tolerance for heterogeneous mixtures and the fact that crystals are not required. Perturbation of subunit interfaces in solution followed by gas-phase detection using mass spectrometry is a current means of probing the disassembly and hence assembly of protein complexes. Herein, we present an alternative method that employs native mass spectrometry coupled with ion mobility and two stages of surface induced dissociation (SID) where protein complexes are dissociated into subcomplexes in the first SID stage. The subcomplexes are then separated by ion mobility and subsequently fragmented into their individual monomers in the second SID stage (SID-IM-SID), providing information on how individual subunits assemble into protein complexes with different native

1  
2  
3 1 topologies. The results also illustrate complex dependent differences in charge redistribution onto individual  
4  
5 2 monomers obtained in SID-IM-SID.  
6  
7  
8 3

## 9 10 4 **Introduction**

11  
12 5 A host of cellular processes are mediated by the formation, and dynamic interaction, of macromolecular  
13  
14 6 complexes.<sup>1, 2</sup> Consequently, characterizing the quaternary structures of protein complexes and their assembly  
15  
16 7 pathways constitutes a necessary step towards the mechanistic understanding of these cellular processes. There  
17  
18 8 are several structural characterization techniques available, such as X-ray crystallography, small-angle X-ray  
19  
20 9 scattering (SAXS), electron microscopy (EM) and nuclear magnetic resonance (NMR) spectroscopy that serve as  
21  
22 10 powerful tools in probing the architecture of protein complexes.<sup>3, 4</sup> However, these approaches are often limited  
23  
24 11 due to the high quantities of sample required, need for very pure samples, and difficulty in studying  
25  
26 12 conformationally dynamic systems.<sup>5</sup> The ability to characterize protein complex disassembly and hence assembly  
27  
28 13 pathways has been greatly aided by the coupling of native mass spectrometry (MS) with ion mobility (IM), which  
29  
30 14 can simultaneously identify the different subcomplexes formed during solution-phase disassembly.<sup>6</sup> This is  
31  
32 15 possible because subcomplexes generated from solution disruption typically resemble the native structures within  
33  
34 16 the intact assembly.<sup>7, 8</sup> The generation of subcomplexes from intact assemblies is also possible in the gas-phase by  
35  
36 17 employing tandem mass spectrometry (MS/MS).<sup>9</sup> However, the most common dissociation method utilized in  
37  
38 18 MS/MS experiments, collision induced dissociation (CID), provides limited direct information on subunit  
39  
40 19 arrangement in the native complex as it typically results in “asymmetric” dissociation into highly charged  
41  
42 20 monomers and complementary (n-1)-mers as the complex undergoes multiple collisions with a neutral gas.<sup>10</sup>  
43  
44  
45

46 21 Alternatively, surface induced dissociation (SID), which involves collision with a surface target, has been  
47  
48 22 shown to yield products reflective of the complex topology, as it allows for the structurally informative, direct  
49  
50 23 dissociation pathways to outcompete the multistep monomer unfolding dissociation pathway.<sup>10</sup> Consequently,  
51  
52 24 prior studies published by the Wysocki group have been successful in utilizing SID as a means of dissociating  
53  
54 25 protein complexes to subcomplexes to facilitate the mapping of subunit contacts within protein complexes,  
55  
56 26 thereby generating direct information on their quaternary structure.<sup>11, 12</sup> Moreover, we have also demonstrated that  
57  
58  
59  
60

1  
2  
3 1 low-energy SID of D<sub>2</sub> homotetramers (complexes with dihedral symmetry<sup>7</sup>) initially results in cleavage of the  
4  
5 2 smaller dimer-dimer interfaces yielding C<sub>2</sub> dimers (complexes with cyclic symmetry) , whereas higher-energy  
6  
7 3 SID results in the secondary cleavage of the larger monomer-monomer interface within the C<sub>2</sub> dimer to produce  
8  
9 4 monomers. These results allowed us to conclude that the SID dissociation pathway (D<sub>2</sub> tetramer → C<sub>2</sub> dimer →  
10  
11 5 monomer) is the reverse of the known assembly pathway.<sup>13</sup> The deconvolution of assembly pathways by SID  
12  
13 6 energy-resolved MS (SID-ERMS) requires monitoring the relative intensities of all SID products (including  
14  
15 7 indirect secondary fragments) obtained from multiple experiments conducted at various SID collision energies  
16  
17 8 and then plotting the relative intensity of the precursor and all products as a function of SID energy producing a  
18  
19 9 SID-ERMS plot. Therefore, although the use of SID-ERMS plots is a relatively straightforward and useful  
20  
21 10 strategy for simple systems such as D<sub>2</sub> homotetramers, interpretation of primary vs. secondary products in these  
22  
23 11 plots becomes more difficult when studying more complex heterogeneous systems from which many possible  
24  
25 12 subcomplexes can be produced and, hence, many possible indirect secondary fragments can also be derived.

26  
27 13 Based on the results described earlier for solution disruption/MS and our single stage SID experiments, we  
28  
29 14 hypothesize that by first generating subcomplexes by SID, followed by IM separation and the direct dissociation  
30  
31 15 of these subcomplexes to individual subunits, it may be possible to probe the relationship between the  
32  
33 16 disassembly and quaternary structure of a protein complex in direct experiments. The present study seeks to test  
34  
35 17 this hypothesis by modifying a quadrupole/IM/time-of-flight (Q/IM/TOF) instrument to incorporate two  
36  
37 18 customized SID devices (before and after the IM chamber) to allow for two stages of SID dissociation followed  
38  
39 19 by detection of the products, after separation, in the TOF. We introduce a method to generate subcomplexes by  
40  
41 20 low energy trap SID (Scheme 1a), which has been shown to proceed via cleavage of the smallest interface(s)  
42  
43 21 within the complexes first. The SID products are then separated by size, shape and charge in IM<sup>14, 15</sup>, following  
44  
45 22 which they can be further dissociated (into individual subunits) by higher energy SID within the transfer region  
46  
47 23 (transfer SID), as shown in Scheme 1b.  
48  
49  
50  
51  
52  
53  
54  
55  
56  
57  
58  
59  
60

## 1 Results and Discussion

2 Three model complexes with different native topologies were chosen for this initial, proof of concept,  
3 investigation: streptavidin, a homotetramer that is a dimer of dimers, tryptophan synthase, a heterotetramer with a  
4 somewhat linear  $\alpha\beta\beta\alpha$  arrangement, and the homopentamer C-reactive protein, which has cyclic symmetry.  
5 Streptavidin (SA) was recently used in our assembly/disassembly studies of D<sub>2</sub> homotetramers described  
6 elsewhere,<sup>13</sup> making it an appealing model system for this SID-IM-SID investigation. The dissociation behavior  
7 observed in trap CID (Figure 1a, tetramer → monomer + trimer) and trap SID (Figure 1b, tetramer → dimer) is  
8 similar to that observed in our previous assembly/disassembly studies involving the SA tetramer<sup>13</sup>. Because trap  
9 CID and SID occur before the IM cell, the different products are separated within the IM cell and hence have  
10 unique drift times, with predicted  $m/z$  of streptavidin subcomplexes given in Table S1. Comparison of the CID-  
11 IM and SID-IM results (Figures 1a and 1b respectively and Table S2) shows several clear differences. The spectra  
12 show the dissociation observed at the energies at which dissociation is first observed, CID 1430 eV and SID 330  
13 eV. A significantly lower energy is required to dissociate the ions with SID in comparison to CID. This is due to a  
14 number of factors, with SID dissociation occurring following a collision event with a massive target (surface) in  
15 which the energy is rapidly deposited. In CID, the ions undergo multiple, stepwise collisions with much smaller  
16 targets (gaseous Ar). This step wise dissociation involves a range of impact parameters and CID thus typically  
17 requires larger lab frame kinetic energies to dissociate ions than does SID. Furthermore, the undissociated +11 SA  
18 tetramer in CID experiments spends a significantly longer time in the IM cell (14.51-19.40 ms) than the native  
19 +11 SA tetramer in MS experiments (10.88-11.79 ms) and has a broader range of drift times, indicative of  
20 unfolding of the SA tetramer in CID. Therefore, these results confirm that the unfolding typically associated with  
21 CID and the corresponding inability to generate informative subcomplexes is responsible for its inability to  
22 directly give information on the quaternary structure of protein complexes. In contrast, the majority of  
23 undissociated SA tetramer from SID-IM has a similar drift time to the native SA tetramer in MS experiments.  
24 However, using single stage SID alone, we cannot completely rule out the possibility that a fraction of the  
25 undissociated tetramers with similar CCS as the original tetramer may be due to the tetramer not colliding with  
26 the surface. Instead, further fragmentation of that undissociated tetramer (see below) is needed, as it may provide

1  
2  
3 1 evidence that the tetramers have been activated by a surface collision. Although the dominant *monomers* in CID  
4 are clearly unfolded (experimental CCS of 17.10 nm<sup>2</sup> (Table S2) vs 15.27 nm<sup>2</sup> expected CCS for a monomer  
5 2  
6 are clearly unfolded (experimental CCS of 17.10 nm<sup>2</sup> (Table S2) vs 15.27 nm<sup>2</sup> expected CCS for a monomer  
7 3  
8 clipped from the crystal structure), the average experimental CCS obtained for the SID *dimer* fragments (20.96  
9  
10 4 nm<sup>2</sup> ± 0.06 nm<sup>2</sup>, Table S2) is similar to the theoretical CCS calculated for the dimers (20.98 nm<sup>2</sup> for a dimer  
11  
12 5 clipped from the crystal structure). Hence, as previously reported, SID results in dissociation patterns that are  
13  
14 6 reflective of the quaternary structure of the native protein complex.<sup>13</sup>  
15

16 7 Next, we employed a second stage of dissociation, either CID or SID, to fragment the products obtained from  
17 8  
18 8 initial SID-IM. Figures 1c (SID-IM-CID) and 1d (SID-IM-SID) represent experiments where primary SID  
19 9  
20 9 products of the +11 SA tetramer (e.g., those obtained in 1b) are separated by IM and allowed to further fragment  
21 10  
22 10 by CID or SID. Because the dimers produced from low-energy trap SID (330 eV) of the +11 SA tetramer are  
23 11  
24 11 formed before the IM cell, they are separated in the IM cell and appear in separate TOF pulses (highlighted by the  
25 12  
26 12 grey diagonal line). However, the fragments produced from transfer CID and SID are formed after the IM, and  
27 13  
28 13 thus appear in identical TOF pulses along with the dimers from which they are generated. Therefore, by taking  
29 14  
30 14 horizontal slices of the mobilogram plots shown in Figures 1c and 1d, we can extract the MS/IM/MS spectra and  
31 15  
32 15 successfully identify the fragments produced from the direct dissociation of the mobility separated dimers and  
33 16  
34 16 undissociated tetramer. It should be noted that in order to extract these data the species have to be well separated  
35 17  
36 17 in IM, in order to obtain the spectra for a single subcomplex. Figures 1e and 1f illustrate extracted spectra  
37 18  
38 18 corresponding to fragmentation of different primary (SID-IM) products, with red (bottom trace) corresponding to  
39 19  
40 19 fragmentation of +7 dimer, green (middle trace) corresponding to fragmentation of +5 dimer, and blue (top trace)  
41 20  
42 20 corresponding to fragmentation of +11 tetramer. It is immediately apparent that the more highly charged +7 dimer  
43 21  
44 21 (7 × 120 V = 840 eV in SID) fragments much more completely than the +5 dimer (5 × 120 V = 600 eV in SID).  
45 22  
46 22 Dissociation of the +7 dimer, which is produced by asymmetric charge partitioning of the initial +11 tetramer  
47 23  
48 23 (+11 tetramer → +7 & +4 dimers) yields +3 and +4 monomers in both SID-IM-CID and SID-IM-SID. In contrast  
49 24  
50 24 the +5 dimer produced by symmetric charge partitioning of the +11 tetramer (+11 tetramer → +6 & +5 dimers)  
51 25  
52 25 yields +2 and +3 monomers, which better correlates with the expected charge state of monomers generated from  
53 26  
54 26 symmetric dissociation of an +11 tetramer (+11/4 monomers = +2.75/monomer). Although both SID-IM-CID  
55  
56  
57  
58  
59  
60

1  
2  
3 1 and SID-IM-SID result in symmetric dissociation of dimers, the energy onset at which dissociation of the +5  
4  
5 2 dimer is observed in CID (Figure 2a, 550 eV) is significantly higher than that in SID (Figure 2b, 300 eV) and the  
6  
7  
8 3 extent of dissociation in CID is much lower. This suggests that SID-IM-SID is a more effective means of directly  
9  
10 4 dissociating subcomplexes (generated in SID-IM) into their individual subunits than SID-IM-CID, as is also  
11  
12 5 shown for the +6 dimer (Figures 1c and 1d).

13  
14 6 Moreover, as illustrated in Figures 1e and 1f (blue spectra) SID-IM-CID of the remaining +11 SA tetramer  
15  
16 7 yields highly charged monomer (+5,+6) and complementary trimer (+6,+5), whereas SID-IM-SID yields  
17  
18 8 predominantly lower-charged dimers (+5,+6) and monomers (+3,+4). Previous studies revealed that high energy  
19  
20 9 SID of the SA tetramer results in primary cleavage to dimers and secondary cleavage of the larger monomer-  
21  
22  
23 10 monomer interface within the dimer to produce monomers.<sup>13</sup> Therefore, we speculate that high abundance of  
24  
25 11 lower-charged monomers is due to the high SID-IM-SID energy (1320 eV for second stage SID). This speculation  
26  
27 12 is further confirmed by the fact that lower energy SID-IM-SID (inset of Figure 1f, 550 eV for second stage SID)  
28  
29 13 of the undissociated +11 SA tetramer from trap SID yields primarily dimer. These results indicate that SID-IM-  
30  
31 14 SID serves as a means of probing the relationship between the disassembly and quaternary structure of a protein  
32  
33  
34 15 complex in more direct experiments than is possible with SID-IM or SID-IM-CID. Based on the streptavidin  
35  
36 16 results, SID-IM-SID offers the distinct advantage of enabling each subcomplex to be interrogated individually  
37  
38 17 within a single experiment and, therefore, can directly confirm the proposed dissociation pathway.

39  
40 18 As noted above, the majority of the undissociated SA tetramer from SID-IM has a drift time similar to that of  
41  
42 19 the native SA tetramer. SID-IM-SID thus provides an opportunity to probe whether the undissociated precursor  
43  
44 20 has indeed collided with the surface. The undissociated tetramer from SID-IM was, therefore, further fragmented  
45  
46 21 in SID-IM-SID over a range of collision energies to determine whether the entire fraction of +11 SA tetramer  
47  
48  
49 22 collides with the surface in single stage SID dissociation. An ERMS plot was generated by extracting the spectra  
50  
51 23 corresponding to the +11 SA tetramer with similar CCS as the original tetramer (TOF pulses: 60-65 bins) and the  
52  
53 24 fraction of remaining precursor was determined. A comparison of the fragmentation efficiency plot generated for  
54  
55 25 the +11 SA tetramer from SID-IM and SID-IM-SID experiments (Figure 2c) clearly illustrates that more SID  
56  
57 26 collision energy is needed to fragment 50% of the undissociated “native-like” SA tetramer in SID-IM-SID (625  
58  
59  
60

1  
2  
3 1 eV for second stage SID) as compared with the unactivated SA tetramer in single-stage SID-IM dissociation (455  
4  
5 2 eV). However, we considered that this increase might also be due to annealing in the IM cell, as the undissociated  
6  
7  
8 3 +11 SA tetramer passes through the IM cell before it can undergo SID-IM-SID. Single stage IM-SID experiments  
9  
10 4 (where the unactivated precursor also passes through the IM cell before SID dissociation) were subsequently  
11  
12 5 conducted to determine the effects of annealing. Although annealing leads to an increase in the SID collision  
13  
14 6 energy needed to fragment 50% of the +11 SA tetramer (510 eV in IM-SID vs. 455 eV in SID-IM), the change is  
15  
16 7 relatively small when compared with that observed in SID-IM-SID (625 vs 455 eV). Therefore, the results  
17  
18 8 confirm that the undissociated +11 SA tetramer has collided with the surface with no significant change in CCS.  
19  
20 9 We speculate that in addition to the conformational changes associated with annealing in the IM cell, the  
21  
22 10 undissociated +11 SA tetramer also undergoes a structural change upon activation (in spite of the lack of change  
23  
24 11 of CCS), which may explain the increase in SID collision energy required for dissociation. We have also seen this  
25  
26 12 behavior in source-activated protein complexes. These changes may be measurable in future if higher resolution  
27  
28 13 IM can be coupled to SID.

29  
30  
31 14 Non-identical subunits can also interact to form heteromeric complexes, and a large fraction of proteins  
32  
33 15 participate in heteromeric protein-protein interactions *in vivo*.<sup>16</sup> Because heteromeric complexes have different  
34  
35 16 types of subunits, the range of quaternary structures they might adopt is greater than is possible for homomeric  
36  
37 17 complexes.<sup>17</sup> However, previous studies published in the literature have demonstrated that the assembly of both  
38  
39 18 homomeric and heteromeric complexes is driven by a hierarchy of interface size, with subcomplexes assembled in  
40  
41 19 the initial stages possessing the largest interfaces.<sup>7, 8</sup> Therefore, we decided to utilize SID-IM-SID to probe the  
42  
43 20 relationship between quaternary structure and disassembly of the model heterotetramer tryptophan synthase (TS).  
44  
45 21 The native topology of the TS tetramer can be described as four subunits arranged in an almost linear fashion to  
46  
47 22 form an  $\alpha\beta\beta\alpha$  complex.<sup>18</sup> In order to determine whether the disassembly of the TS tetramer is driven by a  
48  
49 23 hierarchy of interface size, we first calculated the interfacial surface area of the  $\alpha/\beta$  (1363 Å<sup>2</sup>) and  $\beta/\beta$  (1624 Å<sup>2</sup>)  
50  
51 24 interfaces using PISA analysis.<sup>19</sup> Low-energy SID-IM (570 eV, Figure 3a) of the charge-reduced +19 TS tetramer  
52  
53 25 results in the disruption of the smaller  $\alpha/\beta$  interface to yield  $\alpha$ -monomer and its complementary  $\alpha\beta_2$ -trimer, with  
54  
55 26 predicted  $m/z$  of TS subcomplexes given in Table S3. SID-IM at an intermediate SID collision energy (Figure 3b,  
56  
57  
58  
59  
60

1  
2  
3 1 1330 eV) results in a variety of products that are representative of the quaternary structure of TS. For example, in  
4  
5 2 addition to the dominant products  $\alpha$ -monomer and  $\beta\beta\alpha$ -trimer, the detection of a minor amount of  $\beta_2$ -dimer  
6  
7 3 indicates that the two  $\beta$  subunits are connected. Further, the presence of an  $\alpha\beta_2$ -trimer coupled with the fact that an  
8  
9 4  $\alpha_2$ -dimer is not observed is consistent with the  $\beta_2$ -dimer being flanked by the  $\alpha$  subunits.

10 5 Next, we utilized SID-IM-SID as a means of fragmenting the  $\alpha\beta_2$ -trimer and  $\beta_2$ -dimer with the aim of  
11  
12 6 illustrating that more information can be gained on the assembly of TS tetramer. It is necessary, however, to  
13  
14 7 consider that the  $\alpha\beta_2$ -trimer may not have the same structure as the trimer clipped from the crystal structure, as the  
15  
16 8 CCS of the trimer produced in SID-IM experiments ( $58.83\text{nm}^2$ ) is much smaller than the CCS obtained for the  
17  
18 9 trimer clipped from the crystal structure ( $66.67\text{nm}^2$ ). SID-IM-SID of  $\alpha\beta_2$ -trimer (Figure 3c) produced from initial  
19  
20 10 SID-IM results in the disruption of the other  $\alpha/\beta$  interface yielding  $\alpha$ -monomer and  $\beta_2$ -dimer, consistent with the  
21  
22 11 interfacial analysis in which the  $\alpha/\beta$  was calculated to be smaller than the  $\beta/\beta$  interface. In addition, SID-IM-SID  
23  
24 12 of the  $\beta_2$ -dimer fragment from initial SID-IM results in disruption of the  $\beta/\beta$  interface to produce  $\beta$ -monomers as  
25  
26 13 expected (Figure 3d). It is interesting to note that the experimental CCS of the  $\beta_2$ -dimer ( $47.82\text{ nm}^2 \pm 0.44\text{ nm}^2$ ) is  
27  
28 14 similar although slightly more compact than the theoretical CCS ( $51.22\text{ nm}^2$ ). Consequently, we propose that the  
29  
30 15 assembly of the TS tetramer is a three-step process, where the larger  $\beta/\beta$  interface is formed by the interaction of  
31  
32 16 two  $\beta$  subunits, followed by the association of the  $\alpha$ -monomer and  $\beta_2$ -dimer to form one of the  $\alpha/\beta$  interfaces. The  
33  
34 17 final step involves the binding of another  $\alpha$ -monomer to the  $\alpha\beta_2$ -trimer to form the  $\alpha\beta\beta\alpha$  TS tetramer. The TS  
35  
36 18 assembly pathway proposed here, based upon results of our SID-IM and SID-IM-SID experiments, is in excellent  
37  
38 19 agreement with other descriptions of the self-assembly of the TS complex.<sup>8, 20, 21</sup>

39  
40 20 One difference between the SID-IM-SID results of SA and TS is the charge of the product ions. Streptavidin  
41  
42 21 shows charge conservation with +11 tetramer fragmenting to +6 and +5 dimers, which fragment to +3 and +3 or  
43  
44 22 +3 and +2 monomers, respectively, as expected if charge is conserved on product ions. The initial fragmentation  
45  
46 23 of +19 TS gives +5 to +7  $\alpha$ - monomer and +12 to +14  $\alpha\beta_2$ -trimer, a result that seems reasonable for a  
47  
48 24 heterotetramer. High energy SID of the +12  $\alpha\beta_2$ -trimer in the SID-IM-SID experiment surprisingly leads to two  
49  
50 25 distributions of  $\alpha$ -monomer, one centered around +9 (likely an extended population) and the other at +5  
51  
52 26 (presumably compact). The highly charged monomer is consistent with significant structural rearrangement, or  
53  
54  
55  
56  
57  
58  
59  
60

1  
2  
3 1 unfolding, and charge transfer in the trimer. Previous studies have shown, in a complex dependent manner, that  
4  
5 2 SID product ions can be collapsed, even when folded monomers are produced and even when folded monomers  
6  
7 3 make up a higher order oligomer<sup>22</sup>. The highly charged products may also be due to the high energy second stage  
8  
9 4 of SID used here. In order to further probe the extent of charge conservation in SID-IM-SID an additional protein  
10  
11 5 complex C-reactive protein (CRP) was studied.

12  
13  
14 6 C-reactive protein (CRP) is a cyclic pentameric assembly of identical non-covalently associated subunits,<sup>23</sup> with  
15  
16 7 PISA analysis determining that the interfacial surface area between all monomeric subunits is similar, with  
17  
18 8 predicted  $m/z$  of CRP subcomplexes given in Table S4. Trap SID of the charge-reduced +18 CRP pentamer  
19  
20 9 (Figure 4a) yields primarily monomers and a small amount of all possible subcomplexes (dimers, trimers and  
21  
22 10 tetramers), an SID result that is common for ring-shaped homooligomers. The experimental CCS of the dimers  
23  
24 11 obtained here from trap SID ( $30.09 \text{ nm}^2 \pm 0.35 \text{ nm}^2$ ) is close to the theoretical CCS ( $32 \text{ nm}^2$ ) calculated using two  
25  
26 12 adjacent monomers clipped from the CRP crystal structure (1GNH).

27  
28  
29 13 The “native-like” dimers produced from trap SID of the CRP pentamer were then further fragmented by a second  
30  
31 14 stage of SID, producing monomers with symmetric charge partitioning (Figure 4b). The dissociation of +7 dimer  
32  
33 15  $\rightarrow +3$  & +4 monomers allows us to propose that the dimer comprises two folded monomers, and that the charge is  
34  
35 16 conserved on the individual subunits from pentamer  $\rightarrow$  dimer  $\rightarrow$  monomer. As shown in previous SID-IM  
36  
37 17 studies<sup>24</sup>, the larger protein subunits derived from trap SID of the CRP pentamer in the present study are present  
38  
39 18 as compact, potentially collapsed, structures. Unlike the dimers, the experimental CCS of the trimers obtained  
40  
41 19 from trap SID ( $39.39 \text{ nm}^2 \pm 0.42 \text{ nm}^2$ ) is significantly different from the theoretical CCS ( $46 \text{ nm}^2$ ) calculated using  
42  
43 20 three adjacent monomers clipped from the CRP crystal structure. However, the experimental CCS of the trimers  
44  
45 21 shows a better correlation with the theoretical CCS calculated for the collapsed trimer shown in the inset of Figure  
46  
47 22 4c ( $43 \text{ nm}^2$ ), which was generated by rearranging the monomers into a more compact structure as might be  
48  
49 23 expected of a sub-complex seeking intramolecular charge and structure stabilization. The +11 CRP trimer formed  
50  
51 24 by the initial trap SID of pentamer was subjected to the second stage transfer SID and the fragment ions produced  
52  
53 25 are illustrated in Figure 4c. The presence of both low and high charged monomers suggests that there may be  
54  
55 26 several competing dissociation pathways. For example, the presence of +3 and +4 monomers allowed us to  
56  
57  
58  
59  
60

1  
2  
3 1 speculate that one possible dissociation pathway is: +11 CRP trimer  $\rightarrow$  +3, +4 and +4 monomers. Another  
4  
5 2 possible dissociation pathway is: +11 CRP trimer  $\rightarrow$  +4 monomer and +7 dimer, which may suggest that all the  
6  
7 3 monomer-monomer interfaces in the compact trimer obtained from trap SID are similar. The dissociation  
8  
9 4 pathways show conservation of charges from the initial precursor throughout the SID-IM-SID process, as was  
10  
11 5 seen for SA.  
12  
13

14 6 Interestingly, transfer SID of the +11 CRP trimer also results in asymmetric charge partitioning between  
15  
16 7 monomers and dimers (+11 trimer  $\rightarrow$  +6 monomer & +5 dimer and +11 trimer  $\rightarrow$  +5 monomer & +6 dimer). We  
17  
18 8 speculate that this dissociation pathway is possible because very high SID energies were used and that allows all  
19  
20 9 possible dissociation pathways (including the rearrangement pathway, which leads to the unfolding and ejection  
21  
22 10 of a more highly charged monomer; this pathway may increase in probability when the altered structure trimer  
23  
24 11 collides with the surface).  
25  
26

## 27 12 **Experimental**

28  
29 13 **Chemicals and Reagents.** Streptavidin and recombinant human C-reactive protein from *E. coli* were purchased  
30  
31 14 from Thermo Scientific Pierce Biotechnology (Rockford, IL, U.S.A.). Tryptophan Synthase, ammonium acetate  
32  
33 15 (AA) and triethyl ammonium acetate (TEAA) were purchased from Sigma-Aldrich (St. Louis, MO, U.S.A.). All  
34  
35 16 samples were buffer exchanged into 100 mM ammonium acetate (pH 7) using 6 kDa cut-off Micro Bio-Spin 6  
36  
37 17 columns from Bio-Rad (Hercules, CA, U.S.A.), and analyzed in a 20 mM:80 mM TEAA:AA electrospray buffer.  
38  
39

40 18 **MS Experiments.** All experiments were conducted by utilizing a modified Q-IM-TOF instrument (Synapt G2-S,  
41  
42 19 Waters Corp., Manchester, U.K.) with customized SID devices installed both before and after the IM chamber  
43  
44 20 (see Scheme 1). Typical instrumental conditions are as follows: capillary voltage of 1.0–1.2 kV, cone voltage of  
45  
46 21 20 V, source offset voltage of 20 V, 2.4 mbar gas pressure in the IM cell, a gas flow rate of 120 mL/min into the  
47  
48 22 helium cell and 4 mL/min into trap and transfer regions (in SID experiments- 2mL/min) and a TOF analyzer  
49  
50 23 pressure of  $\sim 6 \times 10^{-7}$  mbar. Wave conditions in the IM cell were wave velocity:  $300 \text{ ms}^{-1}$  and wave height: 20 V.  
51  
52

53 24 **Determination of Collision Cross Section.** The theoretical collision cross section (CCS) values were calculated  
54  
55 25 from crystal structures using the Projection Approximation (PA) model<sup>25</sup> implemented in the open source  
56  
57  
58  
59  
60

1  
2  
3 1 software MOBCAL. The CCS values obtained were corrected as previously described<sup>26</sup> because the PA model  
4  
5 2 typically underestimates CCS by approximately 14%.<sup>27</sup>  
6  
7  
8 3 In a typical ion mobility measurement in the Synapt G2-S instrument, ions from the Trap TWIG are first injected  
9  
10 4 into the IM cell and then separated into 200 bins based on their size, shape or charge. Each bin is subsequently  
11  
12 5 pulsed separately into the TOF analyzer. Because of the non-linear electric field in the IM cell, the experimental  
13  
14 6 CCS has to be externally calibrated rather than using measured drift times to directly calculate them. First the drift  
15  
16 7 times of four standard calibrants (transthyretin, concanavalin A, serum amyloid P and glutamate dehydrogenase)  
17  
18 8 with a mass range that brackets the mass of the analyte were obtained, and a linear calibration curve of the  
19  
20 9 corrected drift time vs. the known CCS is generated. The corrected drift time is then determined for the analyte  
21  
22  
23 10 under identical instrument conditions as used for the standard calibrants, and the experimental CCS of the analyte  
24  
25 11 is determined using the calibration curve.  
26

### 27 12

### 28

### 29 13 **Conclusion**

30  
31 14 In conclusion, SID-IM-SID can be utilized to probe the relationship between quaternary structure and  
32  
33 15 disassembly of protein complexes, with assembly information inferred from the disassembly pathway. We applied  
34  
35 16 this approach to fragment three model systems with different native topologies- a dimer of dimers (SA), a  
36  
37 17 heterotetramer (TS) that is arranged in a linear  $\alpha\beta\beta\alpha$  fashion and a cyclic pentamer C-reactive protein (CRP). The  
38  
39 18 results show how monomers associate to form subcomplexes, which then interact with each other to produce the  
40  
41 19 complete protein complex. Furthermore, charge can be conserved, and tracked, from precursor to products in a  
42  
43 20 complex dependent manner in SID-IM-SID and lack of charge conservation may be indicative of structural  
44  
45 21 rearrangement, although more work is needed in this area.  
46  
47  
48

### 49 22

### 50

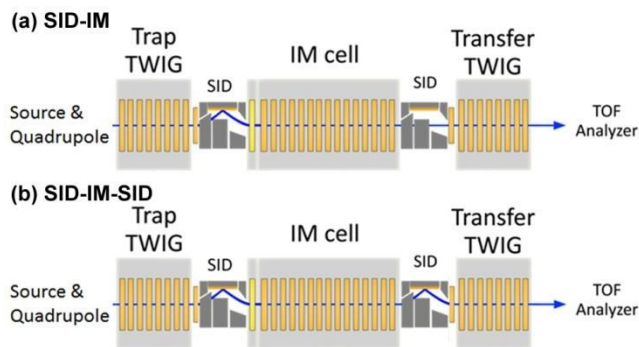
### 51 23 **Acknowledgements**

52  
53 24 We are grateful for financial support from the National Science Foundation (NSF DBI 1455654 to VHW). SRH is  
54  
55 25 supported by a UK Engineering and Physical Sciences Research Council (EPSRC) Doctoral Prize Fellowship.  
56  
57 26 The authors would like to thank Mike Morris and Kevin Giles of Waters Corporation, for helpful discussions in  
58  
59  
60

1  
2  
3 1 implementing SID-SID. We are grateful to Waters Corporation for machining the two SID devices. Mowei Zhou  
4  
5 2 is also thanked for his work in the initial stages of this project.  
6  
7  
8 3  
9

#### 10 4 **References**

- 11
- 12 5 1. L. M. Veenhoff, E. H. M. L. Heuberger and B. Poolman, *Trends in Biochemical Sciences*, 2002, **27**, 242-  
13 6 249.
- 14 7 2. P. Maurice, M. Kamal and R. Jockers, *Trends in Pharmacological Sciences*, **32**, 514-520.
- 15 8 3. D. L. Minor Jr, *Neuron*, 2007, **54**, 511-533.
- 16 9 4. A. B. Ward, A. Sali and I. A. Wilson, *Science*, 2013, **339**, 913-915.
- 17 10 5. C. V. Robinson, A. Sali and W. Baumeister, *Nature*, 2007, **450**, 973-982.
- 18 11 6. H. Hernández and C. V. Robinson, *Nature protocols*, 2007, **2**, 715-726.
- 19 12 7. E. D. Levy, E. B. Erba, C. V. Robinson and S. A. Teichmann, *Nature*, 2008, **453**, 1262-1265.
- 20 13 8. Joseph A. Marsh, H. Hernández, Z. Hall, Sebastian E. Ahnert, T. Perica, Carol V. Robinson and Sarah A.  
21 14 Teichmann, *Cell*, 2013, **153**, 461-470.
- 22 15 9. A. J. R. Heck, *Nat. Methods*, 2008, **5**, 927-933.
- 23 16 10. R. L. Beardsley, C. M. Jones, A. S. Galhena and V. H. Wysocki, *Analytical chemistry*, 2009, **81**, 1347-1356.
- 24 17 11. A. E. Blackwell, E. D. Dodds, V. Bandarian and V. H. Wysocki, *Analytical Chemistry*, 2011, **83**, 2862-2865.
- 25 18 12. M. Zhou, C. M. Jones and V. H. Wysocki, *Anal. Chem.*, 2013, **85**, 8262-8267.
- 26 19 13. Royston S. Quintyn, J. Yan and Vicki H. Wysocki, *Chemistry & Biology*, 2015, **22**, 583-592.
- 27 20 14. A. A. Shvartsburg and R. D. Smith, *Analytical Chemistry*, 2008, **80**, 9689-9699.
- 28 21 15. S. D. Pringle, K. Giles, J. L. Wildgoose, J. P. Williams, S. E. Slade, K. Thalassinou, R. H. Bateman, M. T.  
29 22 Bowers and J. H. Scrivens, *International Journal of Mass Spectrometry*, 2007, **261**, 1-12.
- 30 23 16. K. Tarassov, V. Messier, C. R. Landry, S. Radinovic, M. M. S. Molina, I. Shames, Y. Malitskaya, J. Vogel, H.  
31 24 Bussey and S. W. Michnick, *Science*, 2008, **320**, 1465-1470.
- 32 25 17. T. Perica, J. A. Marsh, S. F. L., E. Natan, L. J. Colwell, S. E. Ahnert and S. A. Teichmann, *Biochemical  
33 26 Society Transactions*, 2012, **40**, 475-491.
- 34 27 18. C. C. Hyde, S. A. Ahmed, E. A. Padlan, E. W. Miles and D. R. Davies, *Journal of Biological Chemistry*, 1988,  
35 28 **263**, 17857-17871.
- 36 29 19. E. Krissinel and K. Henrick, *Journal of Molecular Biology*, 2007, **372**, 774-797.
- 37 30 20. A. N. Lane, C. H. Paul and K. Kirschner, *The EMBO Journal*, 1984, **3**, 279-287.
- 38 31 21. A. Ehrmann, K. Richter, F. Busch, J. Reimann, S.-V. Albers and R. Sterner, *Biochemistry*, 2010, **49**, 10842-  
39 32 10853.
- 40 33 22. M. Zhou, S. Dagan and V. H. Wysocki, *Analyst*, 2013, **138**, 1353-1362.
- 41 34 23. A. K. Shrive, G. M. T. Gheetham, D. Holden, D. A. A. Myles, W. G. Turnell, J. E. Volanakis, M. B. Pepys, A.  
42 35 C. Bloomer and T. J. Greenhough, *Nat Struct Mol Biol*, 1996, **3**, 346-354.
- 43 36 24. M. Zhou, S. Dagan and V. H. Wysocki, *Angewandte Chemie International Edition*, 2012, **51**, 4336-4339.
- 44 37 25. E. Mack, *Journal of the American Chemical Society*, 1925, **47**, 2468-2482.
- 45 38 26. Z. Hall, A. Politis, M. F. Bush, L. J. Smith and C. V. Robinson, *Journal of the American Chemical Society*,  
46 39 2012, **134**, 3429-3438.
- 47 40 27. A. A. Shvartsburg and M. F. Jarrold, *Chemical Physics Letters*, 1996, **261**, 86-91.
- 48
- 49
- 50
- 51
- 52
- 53
- 54 41
- 55
- 56 42
- 57
- 58
- 59
- 60

1  
2  
3 1 **Figures**  
4  
5

2  
3 **Scheme 1.** T-wave region of the modified Waters Synapt G2-S instrument showing the (a) SID-IM and (b) SID-IM-SID experiments.  
4  
5  
6  
7

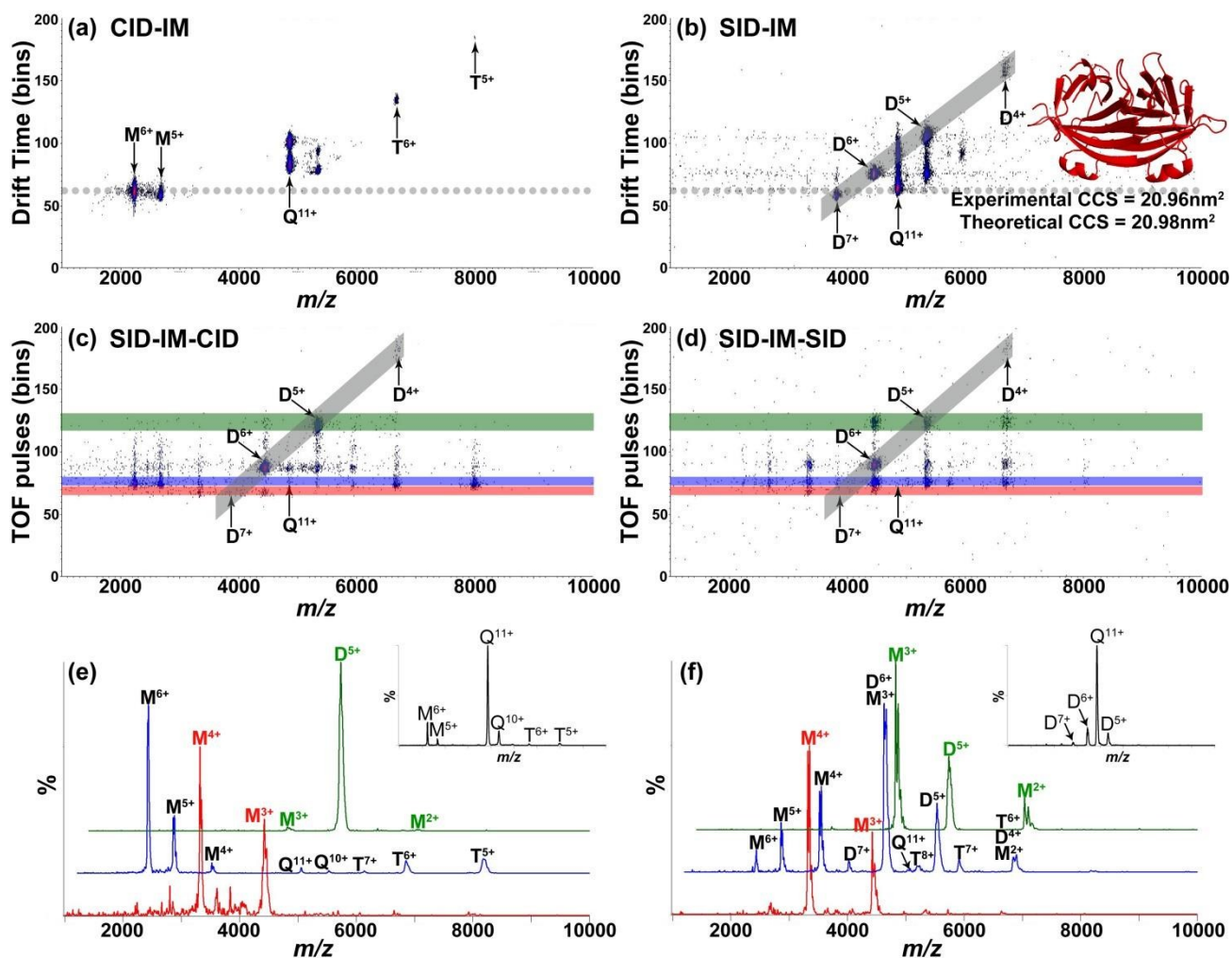


**Figure 1.** Ion mobility mass spectrometry (IM-MS) analysis of a +11 SA tetramer. (a) CID-IM and (b) SID-IM of the +11 SA tetramer at collision energies (CE) of 1430 eV and 330 eV respectively. The crystal structure of the SA dimer expected from dissociation of a D<sub>2</sub> tetramer is shown in the inset of (b). The grey dotted line represents the TOF pulse in which the native +11 SA tetramer appears in MS experiments. Ion mobility mass spectrometry showing the fragments produced in (c) SID-IM-CID and (d) SID-IM-SID experiments are also shown. Trap SID CE is 330 eV, and the transfer CID and SID CEs are 1650 eV and 1320 eV, respectively for tetramer (blue), 1050 eV and 840 eV for +7 dimer (red), and 750 eV and 600 eV for +5 dimer (green). The MS/MS spectra extracted from the highlighted regions of the SID-IM-CID and SID-IM-SID are shown in (e) and (f) respectively. The insets show representative MS/MS spectra from lower energy SID-IM-CID and SID-IM-SID of the remaining +11 SA tetramer from initial SID-IM (CE=330 eV). Extracted MS/MS spectra are color coded to represent their corresponding highlighted regions in the SID-IM-CID/SID mobility mass spectrometry (green (top), blue (middle) and red (bottom) in each case). M, D, T and Q represent monomer, dimer, trimer and tetramer respectively. The ion mobility mass spectrometry plots are shown on a square root scale.

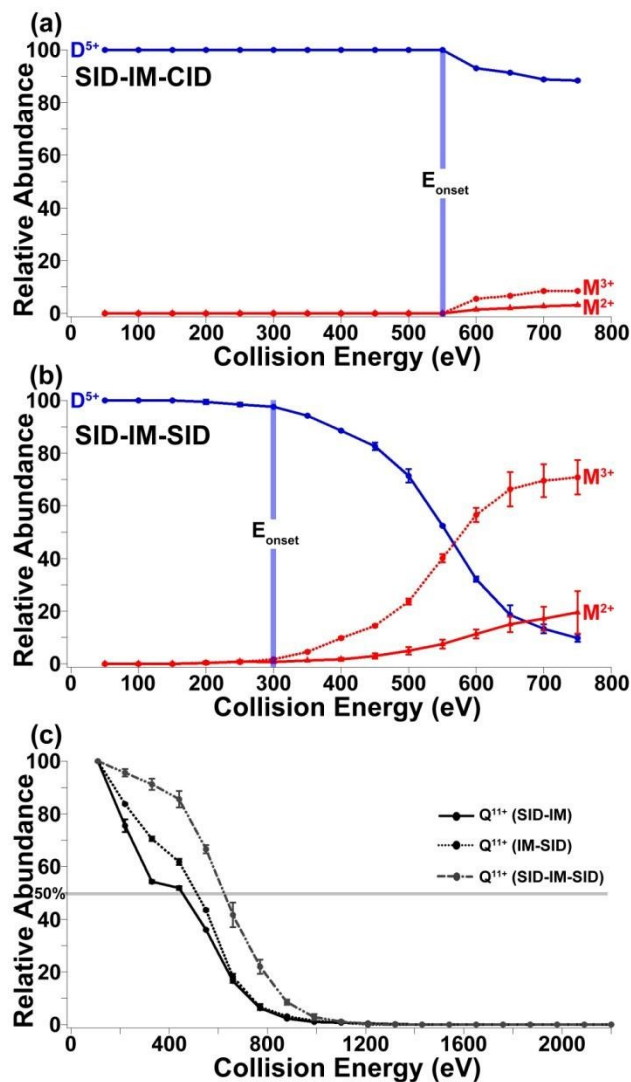


**Figure 2.** (a) SID-IM-CID and (b) SID-IM-SID fragmentation efficiency plot of +5 dimer initially produced from SID-IM of the +11 SA tetramer (CE = 330 eV). (c) SID-IM, IM-SID and SID-IM-SID fragmentation efficiency plots of the +11 SA tetramer. All ERMS plots represent the average from two repeats. The CE of the first stage SID in the SID-IM-SID experiments was 330 eV.  $E_{onset}$  represents the collision energy where dissociation is first observed. M, D and Q represent monomer, dimer and tetramer respectively.

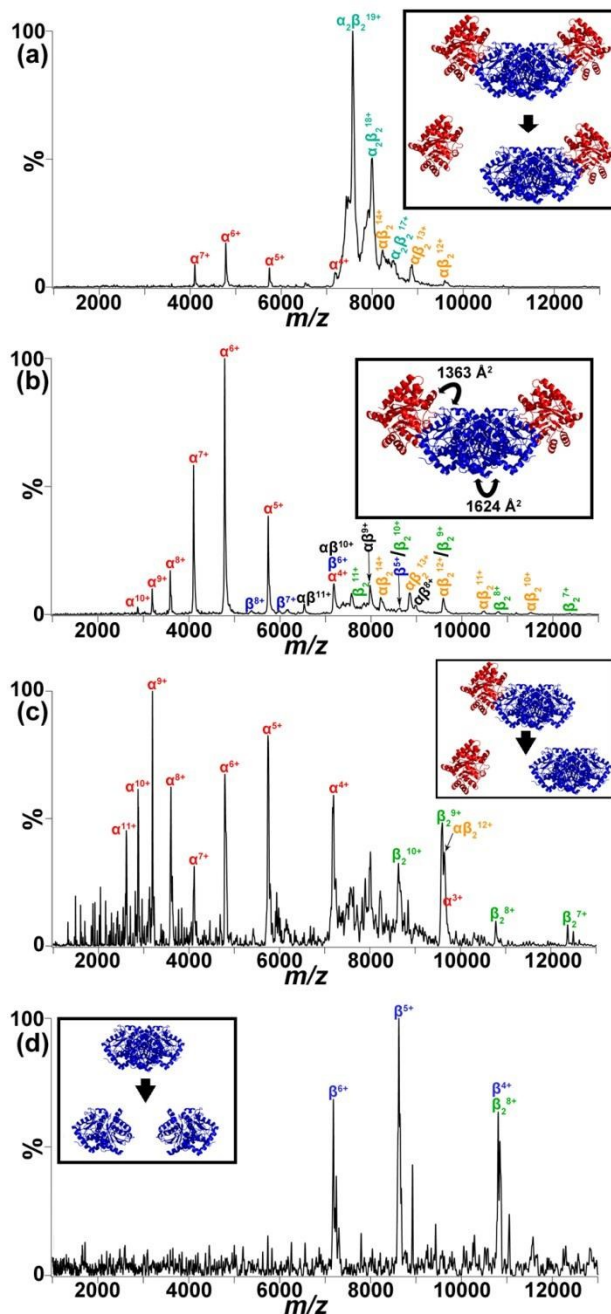


**Figure 3.** (a) SID spectrum showing the different charged fragments produced from the SID-IM of the +19  $\alpha\beta\beta\alpha$  TS tetramer at a collision energy of 1330 eV. The crystal structure of TS (PDB code: 1WBJ) is shown in the inset with its corresponding interfacial areas. SID-IM-SID (CE for second stage SID = 2280 eV) of the (b) +12  $\alpha\beta_2$ -trimer and (c) +8  $\beta_2$ -dimer initially produced from SID-IM (CE = 1330 eV) of the +19  $\alpha\beta\beta\alpha$  TS tetramer. The possible dissociation pathways of the +12  $\alpha\beta_2$ -trimer and +8  $\beta_2$ -dimer are shown in the inset of (b) and (c) respectively.

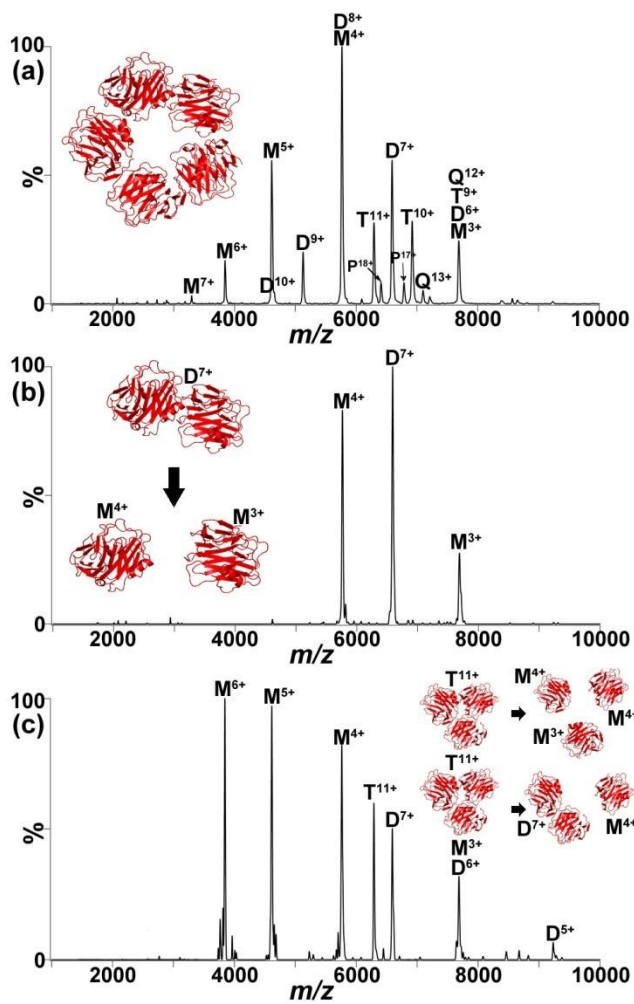


**Figure 4.** (a) SID spectrum showing the different charged fragments produced from the trap SID of the +18 CRP pentamer at a collision energy of 1260 eV. The crystal structure of CRP (PDB code: 1GNH) is shown in the inset. Transfer SID (CE = 2160 eV) of the (b) +7 CRP dimer and (c) +11 CRP trimer produced from trap SID (CE = 1260 eV) of the +18 CRP pentamer. Selected possible dissociation pathways of the +7 dimer and +11 trimer are shown in the inset of (b) and (c) respectively.